JOURNAL OF GEOPHYSICAL RESEARCH, VOL. 104, NO. C1, PAGES 1525–1536, JANUARY 15, 1999

A multiyear hourly sea surface skin temperature data set derived from the TOGA TAO bulk temperature and wind speed over the tropical Pacific

Xubin Zeng, Ming Zhao,[1] Robert E. Dickinson, and Yanping He
Institute of Atmospheric Physics, The University of Arizona, Tucson

Abstract. A theoretical relationship is derived to estimate the sea surface skin temperature from near-surface wind speed and the diurnal variation of sea surface bulk (or bucket) temperature. Coefficients in the relation are determined using the R/V *Franklin* data during the Tropical Ocean-Global Atmosphere (TOGA) Coupled Ocean-Atmosphere Response Experiment (COARE). In contrast to previous methods, surface energy flux data are not explicitly required but rather are implied by the temporal variation of bulk temperature. A multiyear hourly skin temperature data set is obtained using data of bulk temperature at 1-m depth and wind speed from the TOGA Tropical Atmosphere-Ocean (TAO) moored buoys spanning the tropical Pacific Ocean from 95°W in the eastern Pacific to 137°E in the western Pacific between 9°N and 8°S. The diurnal amplitude of skin temperature reaches its maximum of about 2.8 K for daily averaged wind speed between 1–2 m s^{-1} and skin temperature between 20°–21°C and decreases with greater wind speeds. The most frequent amplitude is about 0.5 K, the average amplitude is 0.65 K, and the accumulated frequency for amplitudes greater than 1 K is 10% within the parameter space of daily averaged wind speed between 1 and 15 m s^{-1} and daily averaged skin temperature between 18° and 34°C.

1. Introduction

Sea surface temperatures (SSTs) are necessary for the computation of fluxes of the sensible and latent heat and upward longwave radiation at the air-sea interface. An observational bias in SST would result in changes of the same sign in all these surface fluxes, possibly leading to large errors in the net surface heat flux [*Fairall et al.*, 1996a; *Webster et al.*, 1996]. In addition, the buoyancy flux at the ocean surface is determined by surface heat and freshwater fluxes. Calculation of the surface heat balance in the tropical western Pacific warm pool to an accuracy of 10 W m^{-2} requires an accuracy of 0.3 K in SST [*Fairall et al.*, 1996b].

The term SST has usually referred to the sea surface bulk (or bucket) temperature measured by ships or buoys at a depth of a few centimeters to a few meters, rather than the sea surface skin (or radiometric) temperature. *Webster et al.* [1996] further classified bulk temperature as true bulk temperature (within the upper few centimeters), buoy bulk temperature (typically at 0.5-m depth), and ship bulk temperature (at depths as deep as 5 m) (see *Webster et al.*, 1996, Figure 1). Such distinctions are needed mainly because of the occurrence of two distinct sublayers within the ocean mixed layer. Net cooling at the surface at night gives a skin temperature of 0.1–0.3 K colder [*Wick et al.*, 1996] than ocean under the molecular sublayer of thickness of order of 1 mm [*Grassl*, 1976]. In addition, during the daytime a warm stable lens of water usually occurs within the upper few meters where the bulk of the solar heating is deposited. Since there are very few measurements in the upper few centimeters, we continue to refer to the ship and buoy measurements of temperature as "bulk." However, such temperatures are meaningful during the day only if a depth can be associated with them. The difference between bulk and skin temperatures may have been first measured by *Woodcock* [1940] and was later reviewed by *Katsaros* [1980]. For the region of the Tropical Ocean-Global Atmosphere (TOGA) Coupled Ocean-Atmosphere Response Experiment (COARE) [*Webster and Lukas*, 1992], the difference between skin and bulk temperatures can be larger than 3 K, although it is usually within 1 K [*Fairall et al.*, 1996a].

Various approaches have been developed in the past several decades to understand the difference between

[1]Permanently at Department of Atmospheric Sciences, Nanjing University, Nanjing, 210008, China

Paper number 1998JC900060.
0148-0227/99/1998JC900060$09.00

bulk and skin temperatures [e.g., *Saunders*, 1967; *Price et al.*, 1986; *Schluessel et al.*, 1990; *Soloviev and Schluessel*, 1994, 1996; *Fairall et al.*, 1996a; Kent et al., 1996; Wick et al., 1996]. In particular, *Fairall et al.* [1996a] developed two simple models to correct for the cool skin molecular sublayer (based on the standard *Saunders* [1967] treatment) and the warm daytime stable lens (based on the single-layer version of the model of *Price et al.* [1986]) for the TOGA COARE region. *Kent et al.* [1996], *Soloviev and Schluessel* [1996], and *Wick et al.* [1996] also evaluated extensively the various methods for the difference between bulk and skin temperatures. All these methods require the net surface heat flux and near-surface wind speed. Diurnal averaged precipitation is required in addition for the *Webster et al.* [1996] regression algorithm for the diurnal amplitude of skin temperature.

Ship and buoy observations, however, generally provide only the bulk temperature and environmental conditions (i.e., wind, temperature, and humidity) and not the net heat flux over the diurnal cycle except during field experiments. Consequently, it has not been possible to derive a multiyear skin temperature data over the diurnal cycle for a large region. Polar orbiting satellites in principle estimate skin temperature. However, they cannot give a diurnal cycle, and satellite temperature retrievals from the National Oceanic and Atmospheric Administration (NOAA) advanced very high resolution radiometer (AVHRR) instruments [e.g., *Reynolds and Marsico*, 1993] have been calibrated by means of the bulk temperature from ships or buoys. The difference between skin and bulk temperatures is also important in order to compare bulk temperature measurements with skin temperature retrieved based on radiative transfer models using the along-track scanning radiometer (ATSR) [e.g., *Zavody et al.*, 1995].

This paper develops an algorithm for the computation of skin temperature that uses bulk temperature and wind speed alone (in section 2). With this and bulk temperature and wind speed data over the tropical Pacific Ocean from the TOGA Tropical Atmosphere-Ocean (TAO) moored buoys, we produce a multiyear hourly skin temperature data set. The temporal and spatial distribution of skin temperature, and its relation to environmental conditions, are discussed in section 3, while potential applications are addressed in section 4.

2. Algorithm and Validation

2.1. Algorithm Development

Previous modeling studies [e.g., *Price et al.*, 1986; *Fairall et al.*, 1996a; *Webster et al.*, 1996] have shown how the net surface heat flux and wind speed determine the temporal variation of skin temperature, and also largely the temporal variation of bulk temperature through surface layer mixing. Therefore the temporal variation of the bulk temperature should be highly correlated with the net surface heat flux and hence, along with wind speed, can be used to derive skin temperature.

An accurate relationship between skin and bulk temperatures requires the treatment of oceanic surface energy exchange and details of the oceanic surface mixing layer [e.g., *Price et al.*, 1986; *Kantha and Clayson*, 1994; *Large et al.*, 1994; *Webster et al.*, 1996]. Some scaling guidance, however, is provided by the analytical solution of the vertical heat transfer equation for the near-surface ocean:

$$\frac{\partial T}{\partial t} = K_o \frac{\partial^2 T}{\partial z^2} \tag{1}$$

under an idealistic condition of constant thermal diffusivity, K_o. Assuming the ocean surface temperature at time t is given by $T(0,t) = <T_0> + A\cos(\omega_0 t)$ with $<T_0>$, A, and ω_0 being the mean surface temperature, amplitude, and frequency of the heating, respectively, and neglecting the molecular sublayer, it follows that

$$T(z,t) = <T_0> + az + A\,e^{-bz}\cos[\omega_0(t-cz)]. \tag{2}$$

where a, $b = (\omega_0/2K_o)^{1/2}$, and $c = b/\omega_0$ are constant coefficients.

Equation (2) suggests that the diurnal wave of temperature should have the same shape at different depth but have an amplitude that decreases exponentially and a phase that increases linearly with depth, and that the larger the diffusivity or the lower the frequency of surface heating or cooling, the more slowly the temperature perturbation diminishes with depth. These general features are supported by observations [e.g., *Fairall et al.*, 1996a]. However, the assumptions of a single frequency, constant thermal diffusivity, and absence of a molecular sublayer make (2) unrealistic in detail.

Rather than using (2) directly, we use its functional form to infer an empirical approximation to the actual oceanic diurnal variation, including multiple frequencies, complex mixing processes in the near surface ocean, and the molecular sublayer. This is done through use of the actual diurnal shape of the observed bulk temperature and by allowing the coefficients a, b, and c in (2) to be determined independently by statistical fitting as a function of wind speed, rather than be related directly to a given frequency and eddy mixing coefficient. That is, we assume that

$$T(0,t) = <T_0> + f(t), \tag{3}$$

where, with the bracket denoting a 24 hour averaging, $<T_0>$ is the mean skin temperature for an individual day and f is the variation of temperature around $<T_0>$. Equation (2) is then generalized to infer that the bulk temperature will vary with depth approximately as

$$T(z,t) = <T_z> + e^{-bz}\,f(t-cz), \tag{4}$$

where

$$< T_z > = < T_0 > + az + d \qquad (5)$$

is the mean temperature at depth z for an individual day, and a, b, c, and d are coefficients with the first three being functions of wind speed. The term d is included to capture the daily averaged temperature difference across the molecular sublayer. Equations (4)–(5) mean that the skin temperature can be obtained from the temporal variation of bulk temperature by adjusting the daily mean value (using (5)), diurnal amplitude (through the $\exp(-bz)$ term), and phase (through the $-cz$ term).

Let t_1 and t_2 denote the times when observed skin and bulk temperatures reach their maximum values T_{0max} and T_{zmax}, respectively. The coefficients a, b, c, and d are obtained from observational data by (1) computing d from $< T_z > - < T_0 >$ when wind is sufficiently strong that $< T_z >$ can be assumed to be almost independent of depth in the ocean mixed layer (i.e., the $a\,z$ term in Eq. (5) can be omitted), (2) computing a from Eq. (5), (3) equating c to $(t_2 - t_1)/z$, and (4) computing b as $\ln[(T_{0max} - < T_0 >)/(T_{zmax} - < T_z >)]/z$. Provided the coefficients have been so determined, skin temperature is computed from the bulk temperature at depth z by (1) obtaining $< T_0 >$ from Eq. (5), (2) obtaining $f(t-cz)$ from Eq. (4), (3) linearly interpolating $f(t-cz)$ to $f(t)$ at each hour, and (4) obtaining the skin temperature from Eq. (3).

2.2. Coefficient Determination and Algorithm Validation

Observational data from the R/V *Franklin* during the TOGA COARE period are used to determine coefficients a, b, c, and d. Surface skin temperature was measured by an infrared radiometer installed above the wheelhouse of the ship, pointed at 45° to the ocean surface, and adjusted for surface emissivity and sky reflection. Bulk temperature was measured by the ship's thermosalinograph taking water at a depth of 2.4 m, and wind speed was measured by meteorological sensors on the foremast at 11.3 m above sea level. These and other data (e.g., surface flux) are all available for 27 full days during November 22, 1992 to January 26, 1993, near 2.5°S and 155°E.

Figure 1a shows the bulk versus skin temperature difference as a function of wind speed. The value of d obtained by averaging the temperature difference data for wind speeds greater than 4.5 m s^{-1} is 0.2 K. This value represents the daily mean difference between bulk temperature close to ocean surface (e.g., a few centimeters in the ocean, defined as the "true bulk" temperature by *Webster et al.* [1996]) and skin temperature. The nonbracketed terms in (3)–(4) determine how this temperature difference at a given hour varies with wind and net heat flux in agreement with previous studies [e.g., *Fairall et al.*, 1996a]. The true bulk temperature was not measured by the R/V *Franklin* nor are we aware of any other data sets containing both skin and true bulk temperatures along with wind speed at a nearly fixed location. Therefore it is impossible to verify directly with observations whether or not our assumption of a constant value (0.2 K) for the daily mean of this difference (i.e., d) is globally applicable. However, there has been significant progress in understanding and modeling this skin effect [*Soloviev and Schluessel*, 1994; *Fairall et al.*, 1996; *Wick et al.*, 1996]. By incorporating the skin effect parameterization of *Wick et al.* [1996] into the ocean mixed model of *Kantha and Clayson* [1994], *Webster et al.* [1996] studied effects of radiation, wind, and precipitation on skin temperature diurnal cycle for seven cases representing a range of tropical conditions. Our parameter d for each case can be computed from *Webster et al.* [1996, Table 3], and varies from 0.18 to 0.26 with a mean value of 0.22 K. To the extent that this skin effect parameterization had been validated using tropical and midlatitude data, it provides some justification for assuming an approximately constant value of 0.2 K.

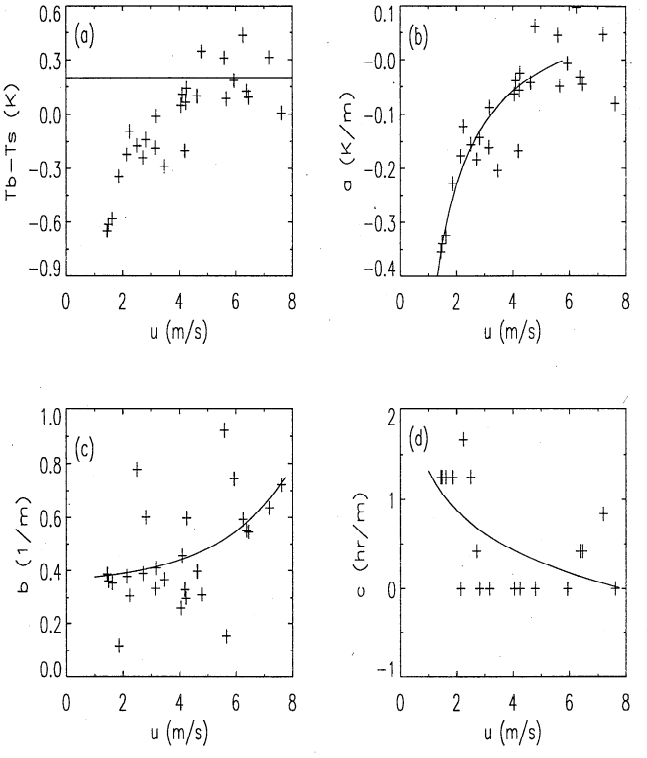

Figure 1. (a) Daily averaged bulk versus skin temperature difference as a function of wind speed at 10 m height determined from the R/V *Franklin* data during the TOGA COARE period with the solid line denoting the value of d in (5) of 0.2 K as the averaged temperature difference for wind speed greater than 4.5 m s^{-1}. Coefficients a, b, and c in (4) and (5) are shown in (b)–(d), respectively, with solid lines representing the best fitted curves. Phase lags (i.e., 2.4c) outside the range of −1 to 5 hours are not used in Figure 1d.

Figures 1b-1d show the coefficients a, b, and c determined using the above 27 days of data. The best fitted curves in the figure can be represented by

$$a = 0.05 - 0.6/u_m + 0.03\ln(u_m), \quad (6)$$

$$b = 0.35 + 0.018\exp(0.4u_m), \quad (7)$$

and

$$c = 1.32 - 0.64\ln(u_m), \quad (8)$$

where u_m is the daily averaged wind speed at 10 m above sea level. Note that the logarithmical and exponential functions, rather than polynomial functions, are used for nonlinear data fitting for simplicity. For convenience, wind speed (u) at height z is converted to that at 10 m by solving the following two equations iteratively:

$$z_o = 0.011u_*^2/9.8 + 1.65 \times 10^{-6}/u_* \quad (9)$$

and

$$u_* = 0.4u/\ln(z/z_o). \quad (10)$$

Equation (9) gives the roughness length for momentum [*Smith*, 1988], and (10) gives the wind stress under neutral conditions. For daily averaged wind speed beyond the range of those observed during the *Franklin* cruise (i.e., 1.5 – 7.6 m s^{-1}), (6)–(8) are still applied but with the following restrictions: $-1.1 < az < 0$, $1 < e^{bz} < 6$, and $0 < cz < 4$.

The fit for c in Figure 1d is not as good as those for a and b in Figures 1b and 1c, because the times when observed skin and bulk temperatures reach their maximum values are both difficult to determine. The variation of coefficients a, b, and c with wind speed as shown in Figures 1b-1d and their physical meanings as implied in (4)–(5) are consistent with the fact that a stronger wind increases oceanic mixing and deepens the surface warm layer, and hence results in reduced mean vertical temperature gradients (in magnitude), more rapid decreases of temperature diurnal amplitude with depth, and reduced temperature phase lags with depth.

Once a, b, c, and d are determined, the bulk temperature at 2.4-m depth and wind speed from the R/V *Franklin* are then used to obtain the skin temperature from (3)–(8), and its comparison with observed values are given in Figure 2. Figure 2d shows that the phase, amplitude, and overall diurnal variation of the derived skin temperature are quite close to observational values except that our algorithm fails to completely capture the observed sharp peaks on December 3 and 5, 1992. Compared with results for the same period given by *Fairall et al.* [1996a, Figure 10] in which net heat flux and wind speed data are used, our results are quite good. The impact of wind, net heat flux, and precipitation on skin temperature can be seen clearly by comparing Figure 2d with Figures 2a-2c. The skin temperature amplitude in Figure 2d decreases at times of increase of wind speed in Figure 2a. The heavy precipitation between December 6–7 seen in Figure 2b is accompanied by a decrease of skin temperature in Figure 2d. The underestimate of maximum skin temperature on December 5 (Figure 2d) is caused by the abrupt change of wind speed and net heat flux (Figures 2a and 2c). However, even using the net heat flux as a direct input, *Fairall et al.* [1996a, Figure 10] also reported the same degree of underestimate. Figure 2e shows the scatterplot of observed and computed hourly skin temperatures for all 27 days. The correlation coefficient is 0.91. The systematic error is negligible (−0.006 K) while the absolute mean deviation is 0.31 K. Figure 2f shows the 27-day averaged diurnal cycle of the observed skin and bulk temperatures and computed skin temperature. Again, the amplitude, phase, and overall variation of computed skin temperature are quite realistic. The averaged amplitude of the bulk temperature is 0.5 K while that of the skin temperature is about 1.2 K (Figure 2f). Therefore Figure 2 demonstrates how our simple algorithm can realistically model the diurnal variation of skin temperature using wind speed and the temporal variation of bulk temperature (which implicitly considers the impact of net heat flux).

To test the robustness of our algorithm, the 27-day data are divided into two subsets of 13 and 14 days of data. The correlation coefficient, bias, and mean absolute deviation between derived and observed skin temperatures are 0.91, −0.06 K, and 0.33 K for the first 13 days and 0.87, 0.04 K, and 0.28 K for the last 14 days. These values from the two subsets agree with each other and with those using all 27 days of data in Figure 2e.

These error estimates do not consider measurement uncertainties. Because the daily average wind speed is used in our algorithm, typical measurement errors of wind speed from ships or buoys as reported by *Fairall et al.* [1996b] and *Weller and Anderson* [1996] (e.g., 0.3 m s^{-1} in root-mean-square error) would not affect our results. The systematic error of up to 0.2 K in observed bulk temperature would introduce the same bias in derived skin temperature through (5), while the root-mean-square error of 0.1 K in bulk temperature would be amplified through the $\exp(b\ z)$ term in (4) which is typically 3 for the hourly R/V *Franklin* data with z = 2.4 m, as shown in Figure 1c. However, this uncertainty in derived skin temperature for a specific day would be significantly reduced in the averaged diurnal cycle, as shown in Figures 2d and 2f. This also implies that the averaged net heat flux error caused by the uncertainty in the derived skin temperature is unlikely to exceed 10 W m^{-2}.

To avoid too weak a diurnal wave relative to measurement errors, it is best to measure the bulk temperature within the upper 2.5 m (or at most 5 m) of the ocean. Bulk temperature measurements at 2.4-m depth for the R/V *Franklin* and at 1-m depth for the buoy data are analyzed in this paper. Another restriction of the approach is that because the diurnal cycle (rather than an instantaneous value) of bulk temperature is used to derive the diurnal variation of skin tem-

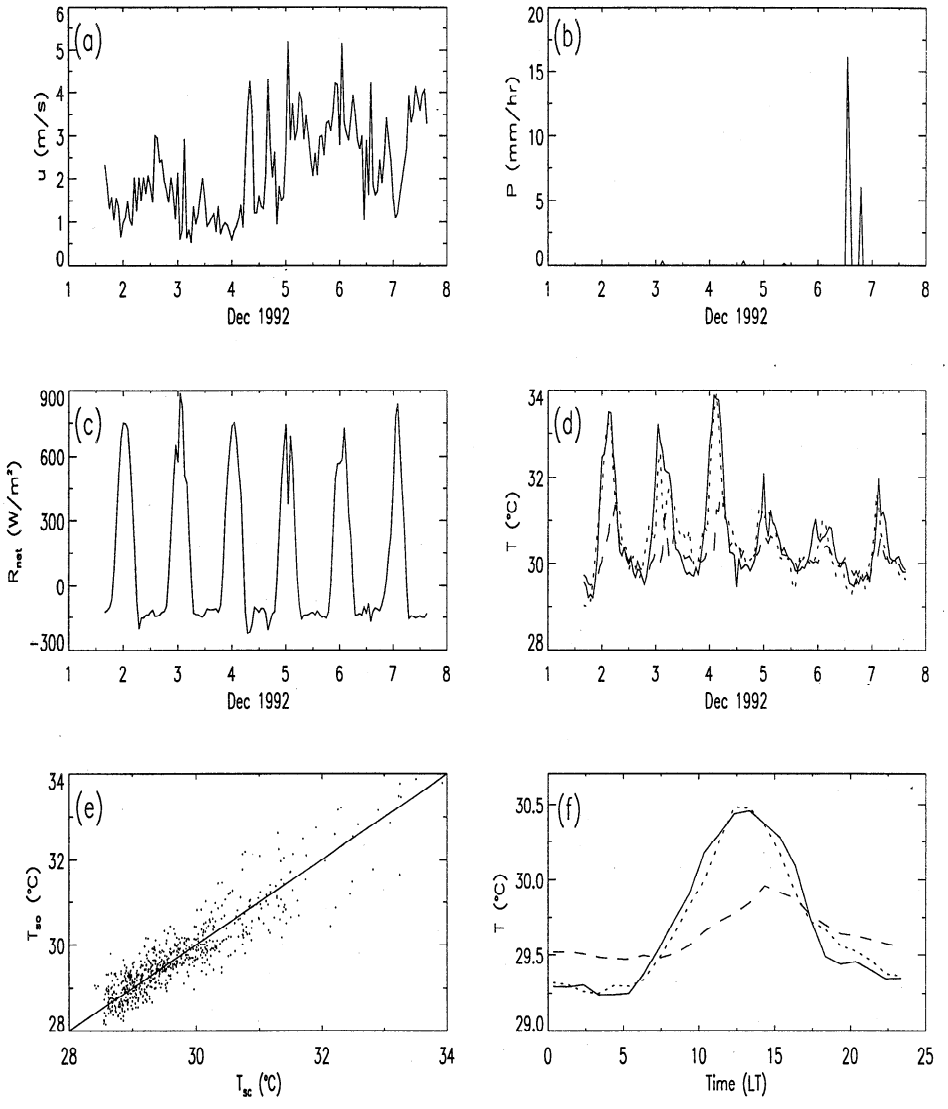

Figure 2. (a) Observed wind, (b) precipitation, (c) net surface heat flux, and (d) sea surface skin temperature from the R/V *Franklin* for 6 days in December 1992. The derived surface skin temperature and observed bulk temperature at a depth of 2.4 m are also given in Figure 2d, denoted by dotted and dashed lines, respectively. (e) Observed skin temperature (T_{so}) from *Franklin* versus the derived values (T_{sc}) for 27 days, and (f) 27-day averaged diurnal cycle of observed and derived temperatures and observed bulk temperature, denoted by the solid, dotted, and dashed lines, respectively, are shown.

perature with the same (but wind speed-dependent) coefficients in (4), bulk temperature should be measured at a nearly fixed location. Therefore this algorithm is better for buoy data than for ship data. However, because the R/V *Franklin* moved slowly (i.e., less than 0.4° of latitude/longitude per day for most of the days) and because the temperature gradient along the ship track over the warm pool is relatively small, the observed diurnal cycle of temperature can still be used to approximately represent values at a fixed location. One implicit assumption in our algorithm derivation is that oceanic mixing is primarily affected by daily mean wind. This places the third limitation: If a transient process associated with precipitation (e.g., a thin fresh layer) or the abrupt and significant change of net heat flux or wind affects surface skin temperature but does not penetrate to the depth for bulk temperature measurement, then its effect would be missing in the derived skin temperature (e.g., on December 3 and 5 in Figure 2d). Another implicit assumption is that the rate of solar absorption with depth is primarily affected by daily mean wind, which places the last limitation: Because this rate varies with optical water type [e.g., *Jerlov*, 1976], application of our algorithm to oceanic regions with different water types (than over the warm pool) may introduce potential errors.

An attempt was made to further evaluate our algorithm using the skin temperature data from the cruise of the R/V *Vickers* extending between 4°N and 4°S from 162°E to 145°W in March 1993 during the Cen-

tral Equatorial Pacific Experiment (CEPEX) [see, e.g., *Wick et al.*, 1996]. However, the rapid movement of the ship (about 4° per day) and the strong meridional temperature gradient over the equatorial Pacific Ocean mean that the observed diurnal cycle of temperature along the track cannot be used to represent values at a fixed location, as required by our algorithm. Therefore this data set would not be useful for our evaluation purposes, though the nighttime skin and bulk temperature at the same time were well utilized by *Wick et al.* [1996].

The Woods Hole Oceanographic Institution (WHOI) surface mooring with an improved meteorological instrument (IMET) measured surface heat flux, wind speed, subsurface temperature at different depths, and other quantities at 1°45′S and 156°E from October 21, 1992 to March 4, 1993, during the TOGA COARE period [*Weller and Anderson*, 1996]. Even though skin temperature was not measured, it is still helpful to use temperature at 1.1-m depth (which is close to the 1-m depth used in section 3) to derive temperature at 0.45-m depth that can then be compared with observed temperature at the same depth. For the 127 days of IMET data, the correlation coefficient, bias, and mean absolute deviation between derived and observed temperature at 0.45-m depth are 0.99, 0.032 K, and 0.056 K, respectively. The smaller scatter of data here than that using the *Franklin* data is expected because the diurnal amplitude of bulk temperature at 0.45-m depth is smaller than that of skin temperature and because the temporal variation of observed bulk temperature is smoother.

We are not aware of suitable observed skin temperature data over other climate regimes (e.g., central and eastern Pacific). Measurements by a floating sea surface temperature sensor during the Tropical Instability Wave Experiment (TIWE) (C.W. Fairall, private communication, 1998) provide perhaps the best available data for an independent evaluation of our algorithm over a different climate regime. The R/V *Wecoma* measured ocean temperature at an effective depth of about 0.05 m using a floating thermistor but did not measure temperature at other depths. Fortunately, *Wecoma* was within about 5 km of one of the TOGA TAO buoys (see section 3) at (0°N, 140°W). Temperatures at

Table 1. Summary of Buoy Data

No.	Site	Duration	Month
1	5n95w	941001 - 960922	17
2	2n95w	921117 - 950126	12
3	0n95w	921001 - 950630	29
4	2s95w	921115 - 960430	34
5	5s95w	940501 - 960530	11
6	8s95w	940815 - 960511	22
7	8n110w	930915 - 960710	19
8	5n110w	930314 - 950331	18
9	2n110w	911101 - 960822	31
10	0n110w	930509 - 950810	19
11	2s110w	911101 - 960930	39
12	5s110w	910409 - 960725	48
13	8s110w	930310 - 960514	38
14	8n125w	930506 - 960915	36
15	5n125w	911208 - 950926	28
16	2n125w	930504 - 950831	22
17	0n125w	921001 - 950630	29
18	2s125w	911105 - 950311	38
19	5s125w	911104 - 950314	35
20	8s125w	931201 - 960814	16
21	9n140w	910502 - 950323	42
22	5n140w	901101 - 960830	34
23	2n140w	930501 - 950321	13
24	0n140w	900501 - 950831	53
25	2s140w	920917 - 950831	34
26	5s140w	901101 - 960831	55
27	8n155w	931101 - 950531	9
28	5n155w	910717 - 950630	36
29	2n155w	920319 - 950331	37
30	0n155w	910721 - 951226	52
31	2s155w	920317 - 960731	27
32	5s155w	910801 - 920217	7
33	8s155w	930306 - 960731	38
34	8n170w	920901 - 951130	29
35	5n170w	920305 - 960724	51
36	2n170w	920901 - 950914	19
37	0n170w	920309 - 960727	53
38	2s170w	920310 - 941130	18
39	5s170w	920822 - 960729	34
40	8s170w	920821 - 941217	15
41	8n180w	931201 - 961110	15
42	5n180w	931201 - 960114	26
43	2n180w	930401 - 960626	31
44	0n180w	940606 - 950331	10
45	2s180w	931201 - 960627	31
46	5s180w	930401 - 950430	20
47	8s180w	931201 - 961024	23
48	8n165e	900906 - 950424	39
49	5n165e	921220 - 950425	29
50	2n165e	920901 - 960126	30
51	0n165e	910401 - 940415	19
52	2s165e	920211 - 960630	28
53	5s165e	940421 - 950430	13
54	8s165e	920901 - 950913	24
55	5n156e	920305 - 960523	20
56	2n156e	930301 - 960229	15
57	0n156e	920302 - 940714	26
58	2s156e	921107 - 940131	6
59	5s156e	910801 - 960328	52
60	5n147e	930206 - 960131	10
61	2n147e	920503 - 960229	14
62	0n143e	920501 - 940430	14
63	2n137e	930501 - 950916	2

Buoys are numbered from the eastern to the western Pacific and from north to south (at a given longitude). Buoy number, location, duration (year, month, and day with each in two digits), and number of months (when no less than 10 days of data are available) are given.

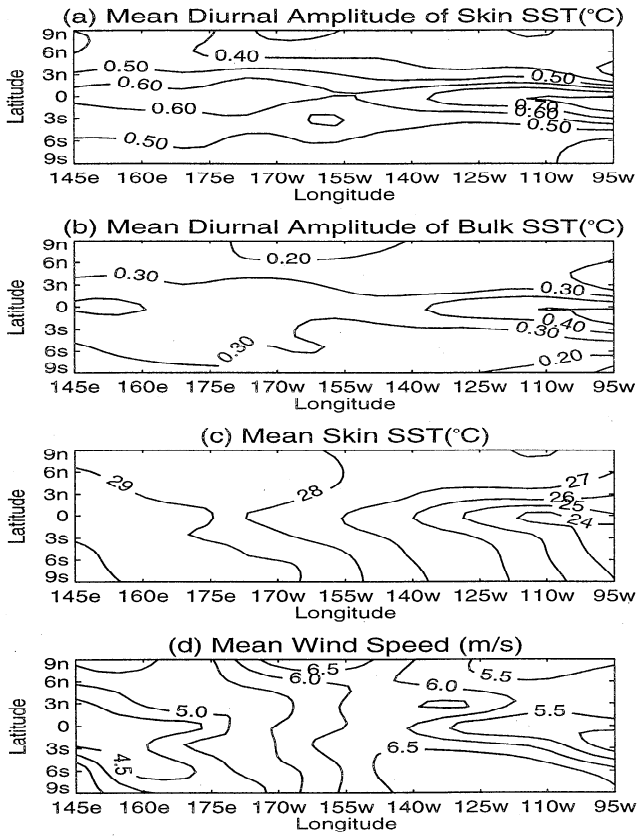

Figure 3. Spatial distribution of amplitudes of the averaged diurnal cycle of (a) derived skin temperature (T_s) and (b) observed bulk temperature (T_b) at a depth of 1 m. (c) Averaged T_s and (d) averaged wind speed are shown.

0.05-m depth can be computed using bulk temperature at 1-m depth and wind data from the TAO buoy measurements. For the 23 days (November 21 – December 13, 1991) of *Wecoma* data, derived values agree with *Wecoma* temperature data very well: The correlation coefficient, bias, and mean absolute deviation between derived and observed temperature at 0.05-m depth are 0.91, 0.015 K, and 0.080 K, respectively.

Furthermore, this applicability issue can be addressed from a different perspective. Theoretically, regardless of climate regimes, skin temperature is determined by net surface heat flux, wind speed, and bulk temperature at a given depth [e.g., *Price et al.*, 1986]. In addition, the temporal variation of bulk temperature can be used to implicitly consider the impact of net heat flux (again regardless of regimes). Because these physical factors have already been included in our algorithm, (4) should be a valid framework over different regimes. Since coefficients in (4) are functions of wind speed alone, the above applicability issue reduces to this question: Given a depth for bulk temperature measurements, are coefficients in (4) nearly independent of net heat flux value (or is the accuracy of our algorithm similar under weak and strong solar insolation conditions)? First, the *Franklin* data are divided into two subsets with the peak solar insolation less (or greater) than 500 W m^{-2} for 5 (or 22) days. The corresponding correlation coefficient, bias, and mean absolute deviation between derived (using bulk temperature at 2.4-m depth) and observed skin temperatures are 0.58, 0.031 K, and 0.20 K (or 0.90, −0.015 K, and 0.33 K). The lower correlation for the low insolation subset is primarily caused by undersampling (5 days only). The IMET data are similarly divided into two subsets for 18 (or 109) days, and the corresponding statistical values between derived (using temperature at 1.1-m depth) and observed temperature at 0.45-m depth are 0.98, 0.018 K, and 0.034 K (or 0.99, 0.034 K, and 0.060 K). These values demonstrate that indeed the accuracy of our algorithm is similar under weak and strong solar insolation conditions.

This issue can also be addressed in terms of the four limitations of our algorithm as discussed earlier. The first two limitations do not apply to the TOGA TAO buoys. The third limitation suggests that derived skin temperature at a given hour has a larger error than averaged diurnal cycle (e.g., for a week). The last limitation does not apply to the equatorial Pacific Ocean because optical water types there are similar [*Jerlov*, 1976]. These tests and arguments suggest that it is not unreasonable to apply our algorithm to the bulk tem-

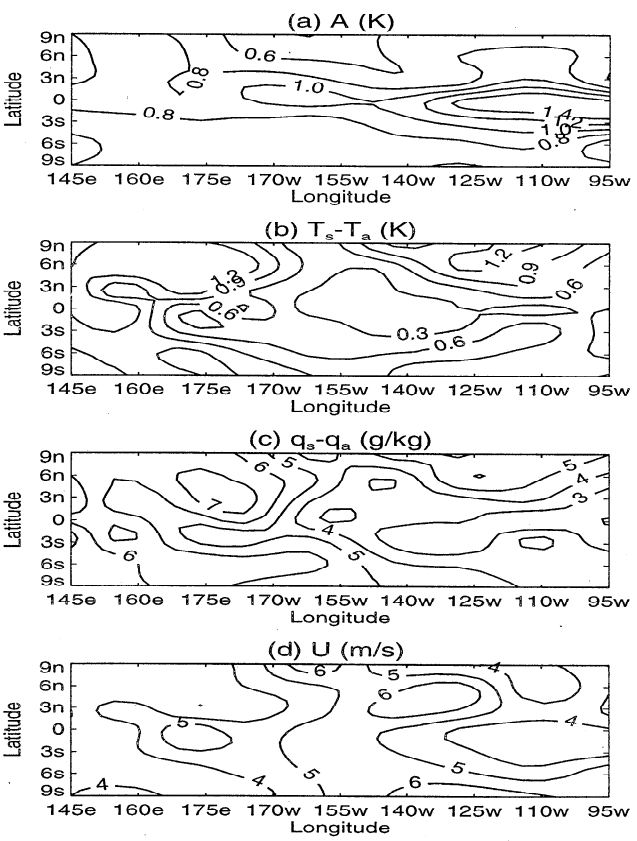

Figure 4. (a) Spatial distribution of the maximum amplitude of monthly averaged diurnal cycle of skin temperature (T_s), (b) the corresponding monthly averaged surface skin versus air temperature difference, (c) surface versus air humidity difference, and (d) wind speed.

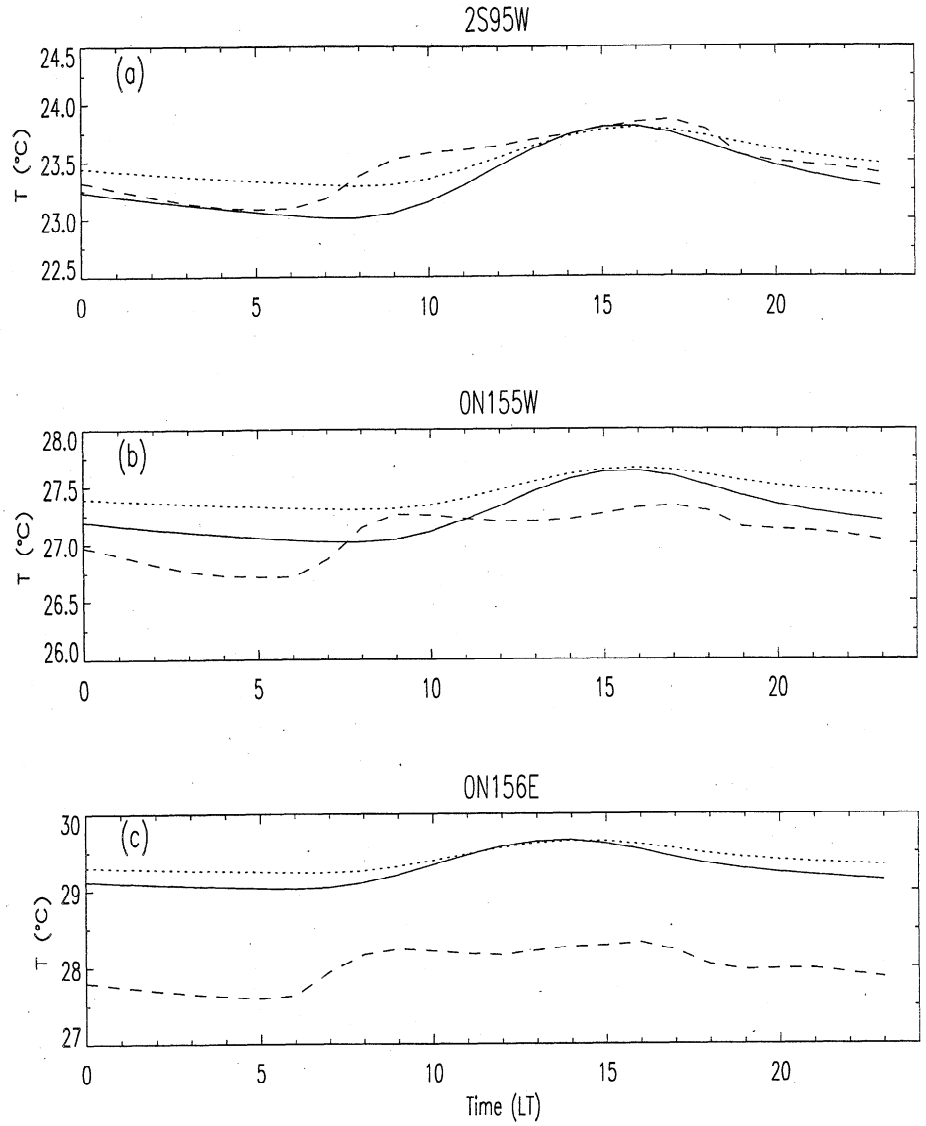

Figure 5. (a) Averaged diurnal cycles of skin, bulk, and air temperatures over the eastern tropical Pacific (2S95W), denoted by the solid, dotted, and dashed lines, respectively, (b) Same as Figure 5a except over the central Pacific (0N155W), (c) Same as Figure 5a except over the western Pacific (0N156E).

perature at 1-m depth over the equatorial Pacific Ocean as done in section 3.

3. A Multiyear Hourly Skin Temperature Data Set

Multiyear hourly data of bulk temperature and wind speed from the TOGA TAO array of moored buoys [*Hayes et al.*, 1991; *McPhaden*, 1993; *Kessler et al.*, 1996] are used here to derive skin temperature. The TAO array of nearly 70 moorings, spanning the equatorial Pacific Ocean from 95°W in the eastern Pacific to 137°E in the western Pacific between 9°N and 8°S. Most of the buoys are the Autonomous Temperature Line Acquisition System (ATLAS) wind and thermistor chain and current meter moorings that measure temperature at 1-m depth and 10 subsurface depths down to 500 m as well as near surface wind at 4 m above the ocean surface and relative humidity and air temperature at 3 m above the surface. Relative humidity and air and ocean temperatures are all sampled every 10 min and averaged hourly, while winds are sampled at a rate of 2 Hz for 6 min centered at the top of each hour, then vector averaged. Even though the use of 6-min wind speed to represent hourly value might be questionable in terms of sampling, the daily averaged wind speed, which is used in our algorithm, is still expected to be unbiased.

We use only data with the standard quality (i.e., predeployment calibration applied) that are available for no less than 10 days in a month. Table 1 shows the location, duration, and number of months when data are available for each of the 63 buoys used in this study. The number of months varies from 2 at 2N137E to 55

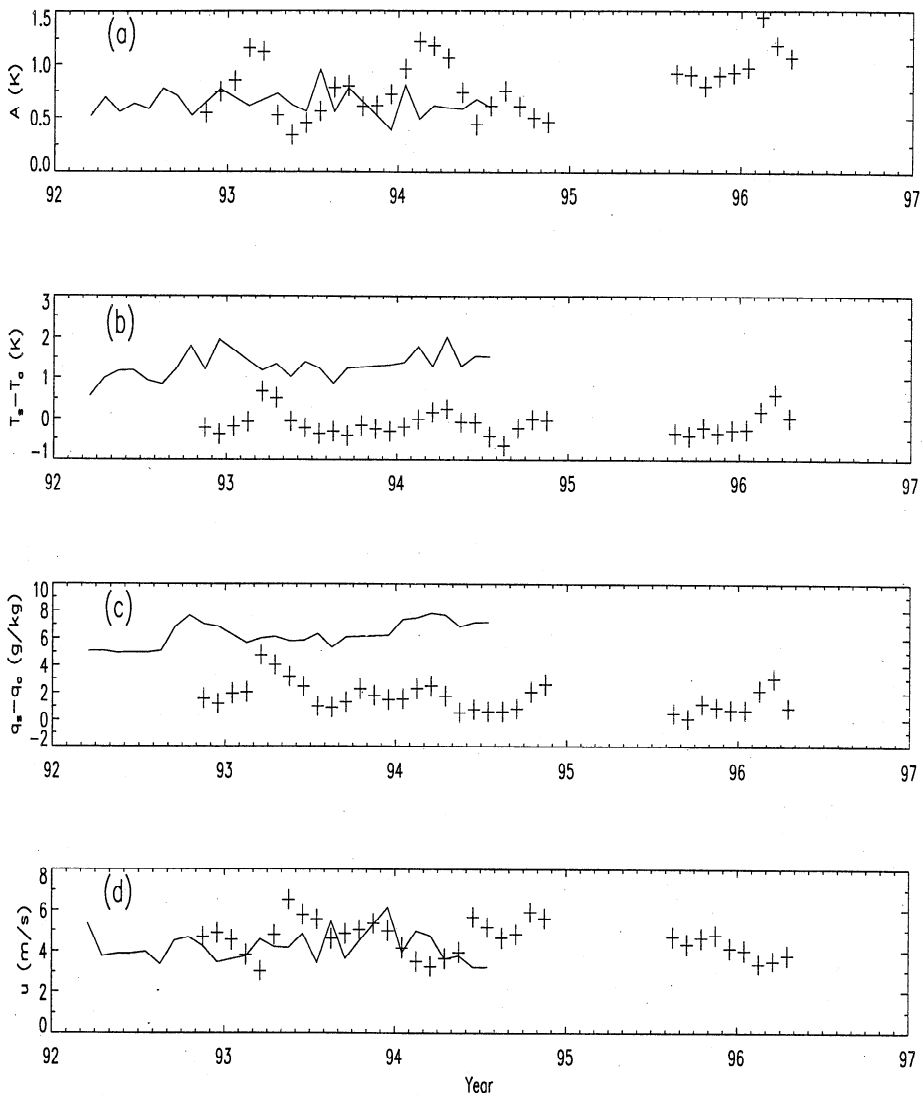

Figure 6. (a) Amplitude of the monthly averaged diurnal cycle of skin temperature (T_s), (b) monthly averaged surface skin versus air temperature difference, (c) surface versus air humidity difference, and (d) wind speed. Results at 0N156E and 2S95W are denoted by the solid lines and plus signs, respectively.

at 5S140W. The earliest starting date is May 1, 1990, at 0N140W while the latest ending date (for data available at the beginning of 1997) is November 11, 1996, at 8N180W.

Figure 3a shows that the amplitude of averaged diurnal cycle of derived skin temperature (T_s) increases toward the Equator and varies from 0.28 to 0.82 K, while that of observed bulk temperature (T_b) at 1-m depth has a similar spatial pattern but smaller amplitudes (from 0.14 to 0.54 K) (Figure 3b). On average, the diurnal amplitude of T_s is about 0.51 K, while that of T_b is 0.30 K. The diurnal amplitude of derived skin temperature is largest over the eastern Pacific (rather than over the western Pacific warm pool) (Figures 3a and 3c) because the diurnal amplitude of observed bulk temperature reaches its maximum there (Figure 3b). However, the ratio of diurnal amplitudes of skin versus bulk temperatures is still larger over the warm pool where wind is weaker on average (Figure 3d).

The monthly averaged diurnal cycle of T_s is computed for each buoy for each month, and the maximum monthly averaged diurnal amplitude among all months available is selected. This maximum amplitude and the averaged environmental conditions for the corresponding month are shown in Figure 4. The amplitude maxima of about 1.5 K that occur over the eastern Pacific (Figure 4a) are associated with small surface skin versus air temperature differences (of about 0.3 K) (Figure 4b), small surface versus air specific humidity differences (of about 2.2 g kg^{-1}) (Figure 4c), and low wind speed (of about 3.4 m s^{-1}) (Figure 4d). In contrast, over the western Pacific, the spatial variation of amplitudes is smaller (Figure 4a), the surface versus air temperature and humidity differences are larger (i.e., the atmosphere

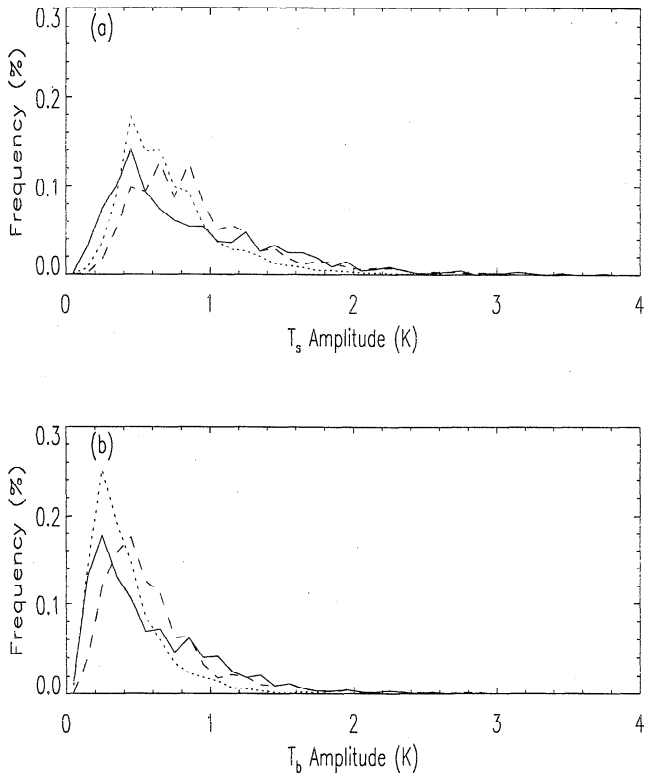

Figure 7. Frequency distribution of diurnal amplitudes of (a) derived surface skin temperature and (b) observed bulk temperature with a bin width of 0.1 K. Results at 0N156E, 0N155W, and 2S95W are denoted by the solid, dotted, and dashed lines, respectively.

is less stable) (Figures 4b and 4c), and wind is weaker on average (but larger than the minimum value over the eastern Pacific) (Figure 4d).

Figure 5 shows the averaged diurnal variations of skin, bulk, and air temperatures at three buoys over the eastern, central, and western equatorial Pacific Ocean, respectively. Over the eastern Pacific (2S95W) (Figure 5a), surface versus air temperature difference is small, and the difference between skin and bulk temperatures leads to positive bulk versus air temperature difference but negative skin versus air temperature difference during most of the nighttime. This implies that the traditional use of bulk temperature (rather than the correct use of skin temperature) could lead to significant errors in the computation of surface sensible and latent heat fluxes. In contrast, over the western Pacific warm pool (0N156E) (Figure 5c), surface versus air temperature difference is quite large so that average stability is not significantly affected by the use of bulk temperature. However, for this region of high surface temperature (of about 29.4°C), surface saturated specific humidity is strongly dependent upon surface temperature through the Clausius–Clapeyron equation at a rate of about 1.5 g kg^{-1} per 1 K. For an average surface versus air humidity difference of 6.3 g kg^{-1} (see Figure 6c) and an average latent heat flux of about 100 W m^{-2} [e.g., *Fairall et al.*, 1996b; *Zeng et al.*, 1998], a difference of 0.42 K between bulk and skin temperatures would lead to 10 W m^{-2} errors in computing latent heat flux (and 2.6 W m^{-2} errors in upwelling longwave radiation). Over the central Pacific (0N155W) (Figure 5b), the use of bulk (rather than skin) temperature would affect the computation of surface fluxes through both the change of stability and surface versus air humidity difference. A more detailed discussion on the impact of surface temperature on surface fluxes is given by *Zeng and Dickinson* [1998].

Figure 6 shows the monthly averaged diurnal amplitude, surface skin versus air temperature and humidity differences, and wind speed for buoys over the eastern and western Pacific Ocean (i.e., 2S95W and 0N156E). The seasonal variation of the monthly averaged skin temperature amplitude is small in the western Pacific but relatively large in the east Pacific with maximum values in boreal spring (see Figure 6a) associated with minimum wind strengths in Figure 6d. The atmosphere at 0N156E is unstable with a large surface versus air humidity difference (about 6.3 g kg^{-1} on average) for each month, while at 2S95W it is stable most of the time with an average surface versus air humidity difference of only 1.7 g kg^{-1} (Figures 6b and 6c).

Figure 7 shows histograms for daily amplitude in 0.1 K intervals at 0N156E, 0N155W, and 2S95W (over western, central, and eastern Pacific Ocean, respectively). The most frequent amplitude for skin temperature T_s is 0.45, 0.45, and 0.65 K at 0N156E, 0N155W, and 2S95W, respectively (Figure 7a), while the corresponding values for bulk temperature are only 0.25, 0.25, and 0.45 K (Figure 7b). The accumulated frequency for T_s amplitudes greater than 1 K is 31% at 0N156E and 2S95W but only 16% at 0N155W (Figure 7a), while the corresponding values for bulk temperature are only 15% (or half of that for T_s) at 0N156E, 11% (or one third of that for T_s) at 2S95W, and 3.5% (or one fifth of that for T_s) at 0N155W (Figure 7b).

Finally, diurnal amplitude of skin temperature is plotted in the parameter space of daily averaged wind speed and skin temperature in Figure 8 using data from all buoys. Figure 8a shows that the maximum amplitude of about 2.8 K is associated with low wind speed and temperature and that amplitudes decrease with wind speed. The averaged amplitude is 0.65 K. The daily averaged skin temperature and wind speed do not exceed 34°C and 15 m s^{-1} at any buoy. Figure 8b shows that wind speed between 5 and 6 m s^{-1} and surface skin temperature between 28° and 29°C occur most frequently, which are associated with diurnal amplitude of 0.5 K in Figure 8a. The accumulated frequency for amplitudes greater than 1 K is about 10%. The accumulated frequency for averaged wind speed greater than 10 m s^{-1} is 0.26%, suggesting that the appearance of very large diurnal amplitudes under strong wind conditions in Figure 8a is caused by undersampling.

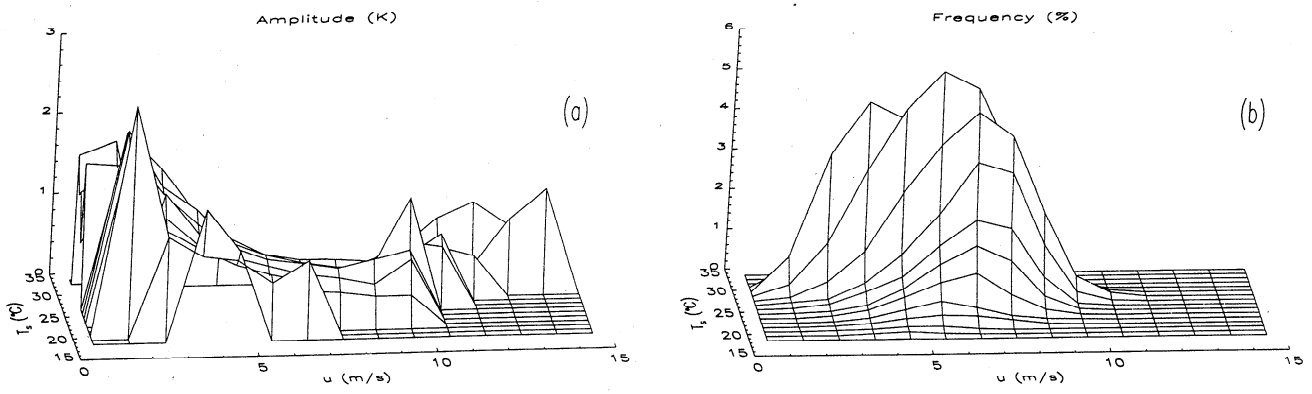

Figure 8. (a) Surface skin temperature diurnal amplitude as a function of daily averaged skin temperature and wind speed and (b) the corresponding frequency distribution. Data from all buoys have been averaged in wind speed and temperature bins with 1 m s^{-1} and 1°C bin widths, respectively.

4. Conclusions

A simple algorithm has been developed for determining the diurnal variation of sea surface skin temperature using near-surface wind speed and the diurnal variation of bulk (or bucket) temperature. In contrast to previous methods, surface energy flux data are not explicitly required but rather are implied by the temporal variation of bulk temperature. Coefficients in the algorithm have been determined using data of 27 days from the R/V *Franklin* during the Tropical Ocean-Global Atmosphere (TOGA) Coupled Ocean-Atmosphere Response Experiment (COARE). The computed skin temperatures agree with observed values with respect to amplitude, phase, and overall pattern. The algorithm has also been validated using 127 days of subsurface temperature at different depths from the IMET buoy during the TOGA COARE period and using 23 days of data from the R/V *Wecoma* over the central Pacific. These independent tests and similar accuracies of the algorithm under strong or weak solar insolation conditions suggest that it may be applicable over different tropical climate regimes. The use of the temporal variation of bulk temperature to infer information about net heat flux makes our algorithm particularly suitable for the analysis of buoy data, and, in certain circumstances, ship data.

Applied to the data of bulk temperature at 1-m depth and wind speed from the TOGA Tropical Atmosphere-Ocean (TAO) buoys, the algorithm provides a multiyear hourly data set of skin temperature across the tropical Pacific Ocean. The maximum amplitude of the averaged skin temperature diurnal cycle over the whole observed period is 0.8 K over the eastern equatorial Pacific with the maximum amplitude of monthly averaged diurnal cycle almost twice as large. The larger amplitudes of derived skin (and observed bulk) temperatures over the cold upwelling region of the eastern Pacific (than over the western Pacific) are primarily caused by higher insolation and reduced trade winds. The spatial and seasonal variations of skin temperature amplitudes are also larger over the eastern than western Pacific. Although the long-term average of bulk temperature at 1-m depth is slightly higher than that of skin temperature, its diurnal amplitude is just 60% of that of skin temperature. Use of bulk temperature (instead of skin temperature) could possibly change the sign of atmospheric stability over the eastern Pacific and affect the surface saturated humidity over the western Pacific.

The diurnal amplitude of skin temperature reaches its maximum of about 2.8 K for daily averaged wind speed between 1 and 2 m s^{-1} and skin temperature between 20° and 21°C. The most frequent amplitude is about 0.5 K, while the averaged amplitude is 0.65 K. The accumulated frequency for amplitudes greater than 1 K is 10%. For the whole data set, the daily averaged wind speed and skin temperature vary between 1 and 15 m s^{-1} and between 18° and 34°C, respectively.

The skin temperature data set introduced here may be useful for a variety of applications in remote sensing (e.g., evaluation of skin temperature retrieved using polar-orbiting and geostationary satellite instruments), data analysis (e.g., the impact of daily and monthly averaging on surface flux computations, the relation of surface latent heat fluxes to wind speed, and the relation of skin temperature to boundary layer process, clouds and radiation, and precipitation), and numerical modeling (e.g., the impact of skin temperature diurnal cycle on atmospheric modeling).

However, it needs to be emphasized that this algorithm has several limitations: Bulk temperature should be measured within the upper 2.5 m (or at most 5 m) of the ocean; its diurnal variation should be measured at a nearly fixed location; the derived skin temperature data will only show the effects of wind, heat fluxes, and precipitation that significantly affect the bulk temperature; and the algorithm can be applied with more

confidence over oceanic regions with optical water type similar to that over the warm pool (or type I, IA, or IB in *Jerlov* [1976]). Furthermore, this algorithm can only be used to derive skin temperature if a time series of bulk temperature measurements are available. The need to further evaluate this algorithm over the eastern Pacific and test its applicability outside of the equatorial Pacific requires observational data.

Acknowledgments. This work was supported by the NOAA OGP under grant NA66GP0179 and NSF under grant ATM-9419715. C.W. Fairall is thanked for providing the R/V *Wecoma* data. R.W. Reynolds and two anonymous reviewers are thanked for their insightful and helpful comments that lead to a significant improvement of the paper. The R/V *Franklin* data, IMET data, and TOGA TAO data were obtained via the Internet and were prepared by E.F. Bradley, R.A. Weller, and the TOGA TAO Office of the Pacific Marine Environmental Laboratory, respectively.

References

Fairall, C.W., E.F. Bradley, J.S. Godfrey, G.A. Wick, and J.B. Edson, Cool-skin and warm-layer effects on sea surface temperature, *J. Geophys. Res.*, *101*, 1295-1308, 1996a.

Fairall, C.W., E.F. Bradley, D.P. Rogers, J.B. Edson, and G.S. Young, Bulk parameterization of air-sea fluxes for Tropical Ocean-Global Atmosphere Coupled-Ocean Atmosphere Response Experiment, *J. Geophys. Res.*, *101*, 3747-3764, 1996b.

Grassl, H., The dependence of the measured cool skin of the ocean on wind stress and total heat flux, *Boundary Layer Meteorol.*, *10*, 465-474, 1976.

Hayes, S.P., L.J. Mangum, J. Picaut, A. Sumi, and K. Takeuchi, TOGA-TAO: A moored array for real-time measurements in the Tropical Pacific Ocean, *Bull. Am. Meteorol. Soc.*, *72*, 339-347, 1991.

Jerlov, N.G., *Marine Optics*, 231 pp., Elsevier, New York, 1976.

Kantha, L.H., and C.A. Clayson, An improved mixed layer model for geophysical applications, *J. Geophys. Res.*, *99*, 25,235-25,266, 1994.

Katsaros, K.B., Radiative sensing of sea surface temperature, *Air-Sea Interaction: Instruments and Methods*, edited by F. Dobson, L. Hasse, and R. Davies, 801 pp., Plenum, New York, 1980.

Kent, E.C., T.N. Forrester, and P.K. Taylor, A comparison of oceanic skin effect parameterizations using shipborne radiometer data, *J. Geophys. Res.*, *101*, 16,649-16,666, 1996.

Kessler, W.S., M.C. Spillane, M.J. McPhaden, and D.E. Harrison, Scales of variability in the equatorial Pacific inferred from the Tropical Atmosphere-Ocean buoy array, *J. Clim.*, *9*, 2999-3024, 1996.

Large, W.G., J.C. McWilliams, and S.C. Doney, Oceanic vertical mixing: A review and a model with a nonlocal boundary layer parameterization, *Rev. Geophys.*, *32*, 363-403, 1994.

McPhaden, M.J., TOGA-TAO and the 1991-1993 El Nino-Southern Oscillation event, *Oceanogr.*, *6*, 36-44, 1993.

Price, J.F., R.A. Weller, and R. Pinkel, Diurnal cycling: Observations and models of the upper ocean responses to diurnal heating, cooling, and wind mixing, *J. Geophys. Res.*, *91*, 8411-8427, 1986.

Reynolds, R.W., and D.C. Marsico, An improved real-time global SST analysis, *J. Clim.*, *6*, 114-119, 1993.

Saunders, P.M., The temperature at the ocean–air interface, *J. Atmos. Sci.*, *24*, 269-273, 1967.

Schluessel, P., W.J. Emery, H. Grassl, and T. Mammen, On the bulk-skin temperature difference and its impact on satellite remote sensing of the sea surface temperature, *J. Geophys. Res.*, *95*, 13,341-13,356, 1990.

Smith, S.D., Coefficients for sea surface wind stress, heat flux, and wind profiles as a function of wind speed and temperature, *J. Geophys. Res.*, *93*, 15,467-15,472, 1988.

Soloviev, A.V., and P. Schluessel, Parameterization of the cool skin of the ocean and of the air-ocean gas transfer on the basis of modeling surface renewal, *J. Phys. Oceanogr.*, *24*, 1339-1346, 1994.

Soloviev, A.V., and P. Schluessel, Evolution of cool skin and direct air-sea gas transfer coefficient during daytime, *Boundary Layer Meteorol.*, *77*, 45-68, 1996.

Webster, P.J., and R. Lukas, TOGA COARE: The coupled ocean-atmosphere response experiment, *Bull. Am. Meteorol. Soc.*, *73*, 1377-1416, 1992.

Webster, P.J., C.A. Clayson, and J.A. Curry, Clouds, radiation, and the diurnal cycle of sea surface temperature in the Tropical Western Pacific, *J. Clim.*, *9*, 1712-1730, 1996.

Weller, R.A., and S.P. Anderson, Surface meteorology and air-sea fluxes in the western equatorial Pacific warm pool during the TOGA Coupled Ocean-Atmosphere Response Experiment, *J. Clim.*, *9*, 1959-1990, 1996.

Wick, G.A., W.J. Emery, L.H. Kantha, and P. Schluessel, The behavior of the bulk-skin sea surface temperature difference under varying wind speed and heat flux, *J. Phys. Oceanogr.*, *26*, 1969-1988, 1996.

Woodcock, A.H., Convection and soaring over the open sea, *J. Mar. Res.*, *3*, 248, 1940.

Zavody, A.M., C.T. Mutlov, and D.T. Llewellyn-Jones, A radiative transfer models for sea surface temperature retrieval for the along track scanning radiometer, *J. Geophys. Res.*, *100*, 937-952, 1995.

Zeng, X. and R.E. Dickinson, Impact of diurnally-varying skin temperature on surface fluxes over the tropical Pacific, *Geophys. Res. Lett.*, *25*, 1411-1414, 1998.

Zeng, X., M. Zhao, and R.E. Dickinson, Intercomparison of bulk aerodynamic algorithms for the computation of sea surface fluxes using the TOGA COARE and TAO data, *J. Clim.*, *11*, 2628-2644, 1998.

X. Zeng, R.E. Dickinson, and Y. He, Institute of Atmospheric Physics, The University of Arizona, Tucson, AZ 85721. (e-mail: xubin@gogo.atmo.arizona.edu; robted[or yanping]@stratus.atmo.arizona.edu)

M. Zhao, Department of Atmospheric Sciences, Nanjing University, Nanjing, 210008, China.

(Received November 18, 1997; revised September 28, 1998; accepted October 23, 1998.)